POLARIMETRIC PASSIVE REMOTE SENSING OF OCEAN WIND VECTORS

S. H. Yueh, R. Kwok, F. K. Li, S. V. Nghiem and W. J. Wilson

Jet Propulsion Laboratory

California Institute of Technology

4800 Oak Grove Drive

Pasadena, CA 91109

J. A. Kong

Research Laboratory of Electronics

Massachusetts Institute of Technology

77 Massachusetts Avenue

Cambridge, MA 02139

Submitted to Journal of Geophysical Research

April 1993

Abstract

This paper investigates the theory of polarimetric passive remote sensing of wind-generated sea surfaces and the potential application of polarimetric radiometry to ocean surface winds. The small perturbation method (SPM), derived to second order, is applied to the Stokes vectors of the thermal emission from random rough dielectric surfaces described by anisotropic directional spectra. To verify the accuracy of the SPM, a Monte Carlo simulation is performed to calculate the Stokes vectors of the emission from the simulated one-dimensional random rough surfaces with a power-law spectrum for various observation angles and surface parameters. The theoretical results of the SPM for all four Stokes parameters are in excellent agreement with the numerical results obtained from the Monte Carlo simulation. Moreover, the second-order coherent fields are indispensible in the theoretical evaluation of the third and fourth Stokes parameters. Otherwise, the reflectivities of random rough surfaces would be significantly over-estimated, and the signs of the third and fourth Stokes parameters would be incorrect. The SPM is then applied to small-scale sea surfaces described by an empirical surface spectrum. Theoretical model functions of the Stokes parameters are illustrated, and the inversion of surface wind vectors from polarimetric brightness data is investigated. The results indicate that polarimetric radiometry allows wind vector measurements with only one azimuthal observation angle, which is made possible by the different azimuthal dependence between the third Stokes parameter and the first two Stokes parameters. Radiometers with a single-azimuth-observation design will not only simplify the antenna-beam-scanning mechanism, but also will be free from the complexity associated with the data co-registration required for multiple-azimuth-observation designs.

1. Introduction

There has been an increasing interest in the microwave passive polarimetry of geophysical media [Tsang, 1991]. Theoretical calculations for the Stokes parameters of the thermal emission have been presented for one-dimensional periodic dielectric surfaces in [Veysoglu et al., 1993], and for one-dimensional ocean-like rough surfaces with a prescribed power-law spectrum in [Yueh and Kwok, 1992a; Johnson et al., 1993]. The theoretical predictions were verified by the measured Stokes parameters of thermal emission from periodic soil surfaces at X band [Nghiem et al., 1991], and measurements over water surfaces impressed with a fiberglass layer with a sinusoidal profile at Ku band [Yueh et al., 1992] and at X band [Johnson et al., 1992]. All the results show that the Stokes parameters are functions of the azimuth angle between the observation direction and the corrugation direction of surfaces. However, further analysis and experiments are necessary for two-dimensional rough surfaces.

Recently, it has been shown by Etkin et al. [1991] and Wentz [1992] that the brightness temperatures of horizontal and vertical polarizations, T_h and T_v, of ocean surfaces vary as functions of the azimuth angles. Etkin et al. found the dependence of brightness temperatures on the azimuth angle during circle flights using their aircraft radiometers for grazing angle ($\theta = 78°$) observations with $\lambda = 1.5$ cm and nadir viewing with $\lambda = 0.8$, 1.5, and 8 cm. It was observed that the directional dependence rapidly dropped with increasing electromagnetic wavelength. However, the measurements were not made for the middle range of incidence angles, which is important for spaceborne applications when spatial coverage and resolution need to be considered together. In the results published by Wentz [1992], the data investigated were collected by the Special Sensor Microwave/Imager (SSM/I), which is not capable of measuring the third Stokes parameter. After being co-

registered with the buoy-measured wind vector, T_h and T_v at both 19 and 37 GHz were found to be dependent on wind direction. The results indicate that the directional feature of water surfaces contributes to the azimuthal variation of brightness temperatures.

Besides the above reported observations for T_h and T_v, Dzura et al. [1992] presented the first evidence of the azimuthal variation of polarimetric brightness temperatures of sea surfaces, though the measurements were made at normal incidence and only one case was presented. Figure 5 in their paper showed that when the second Stokes parameter (Fig. 5b) reached maximum, the third Stokes parameter (Fig. 5c) was nearly zero, and vice versa. No explanation was provided in their paper for this observed signatures, whereas in this paper we show that for nadir observations the second and third Stokes parameters should behave like $\cos 2\phi$ and $\sin 2\phi$, respectively, which well explain the reported azimuthal signatures. However, since only one example was reported, and since the results were collected at nadir observation angles, more extensive experiments and analyses of the azimuthal variations of the Stokes parameters over wind speeds and incidence angles are required to evaluate the applicability of polarimetric radiometry to ocean surface winds.

In view of the recent observations, a theoretical analysis based on the SPM is presented in this paper to extend the theoretical calculations to two-dimensional random rough surfaces to evaluate the contribution to polarimetric emissivities from the small-scale sea surfaces (capillary waves), which are the source of the Bragg scattering at microwaves. The SPM has been used previously to derive the sea surface emission at microwaves by Wu and Fung [1972] for isotropic random rough surfaces. However, their theory predicted no azimuthal dependence of brightness temperatures because the surface spectrum was assumed to be isotropic. Furthermore, the third and fourth Stokes parameters are expected to be zero from their theory, unlike the results presented in this paper where we generalize

the theory to random surfaces with anisotropic wavenumber spectra. Additionally, the accuracy of the SPM for surface emission is evaluated with results obtained from a Monte Carlo simulation technique for one-dimensional rough surfaces. This comparison has not been presented in the literature to the authors' knowledge, though quite a lot of work has been done in verifying the SPM for ocean surface scattering in active remote sensing. Finally, we investigate the application of polarimetric radiometry for the retrieval of ocean wind field. The SPM is applied to the small-scale sea surfaces for developing the appropriate form of the model function of the Stokes vector for sea surface emission. We show that it is possible to retrieve the wind vector using polarimetric radiometers with only one azimuthal observation angle (to be referred to as a "single-look polarimetric radiometers"), as opposed to the two or more azimuthal observation configuration proposed by Wentz [1992] with radiometers measuring only the first two Stokes parameters T_h and T_v. The single-look design only requires a simple antenna-beam-scanning mechanism, like that of SSM/I, and does not have the complexity of data co-registration required for multi-look systems.

In Section II, the theory of polarimetric radiometry is summarized and a polarimetric version of Kirchhoff's law is presented to relate the Stokes vector to the polarimetric bistatic scattering coefficients. Section III summarizes the results of the SPM derived to second order for rough surfaces with anisotropic directional spectra. Section IV compares the results of the SPM with the Monte Carlo simulation technique for the polarimetric emission from one-dimensional random rough surfaces characterized by a power law spectrum at various observation angles. In Section V, the SPM is applied to the Stokes vectors of thermal emission from the small-scale wind-generated sea surfaces described by an empirical wavenumber spectrum for various wind speeds at an SSM/I frequency. Section VI discusses issues related to polarimetric radiometry for the ocean-wind-vector retrieval

using only data with one azimuth look. Section VII summarizes the results of this paper and discusses the remaining issues regarding the application of polarimetric radiometry for ocean wind vector retrieval.

II. Polarimetric radiometry

For microwave polarimetric radiometry, thermal emission is described by a Stokes vector with four parameters

$$I_s = \begin{bmatrix} T_h \\ T_v \\ U \\ V \end{bmatrix} = c' \begin{bmatrix} < E_h E_h^* > \\ < E_v E_v^* > \\ 2Re < E_v E_h^* > \\ 2Im < E_v E_h^* > \end{bmatrix} \qquad (1a)$$

where E_h and E_v are the horizontally and vertically polarized components of electric fields as illustrated in Figure 1. The definitions of the h-pol, v-pol, and wave vectors are the same as those used in [Yueh et al., 1988]. The angular brackets denote the ensemble average of the argument, and c' is a proportional constant [Yueh and Kwok, 1992 b]

Besides the above definition, an alternative definition of the Stokes vector has also been widely used in remote sensing [Tsang et al., 1985]:

$$I_s' = \begin{bmatrix} I \\ Q \\ U \\ V \end{bmatrix} = \begin{bmatrix} T_v + T_h \\ T_v - T_h \\ U \\ V \end{bmatrix} \qquad (1b)$$

Both definitions contain exactly the same information. However, this definition will render a convenient representation in illustrating the emission from small-scale sea surfaces at near nadir observation angles in Section VI.

For the development of geophysical model functions for spaceborne sensors, which relate the emission parameters to the geophysical signatures, the Stokes parameters are

usually expressed in the Fourier series of the azimuth angle ϕ. For wind-generated sea surfaces, which are our focus in this paper, reflection symmetry is expected for the surfaces with respect to the symmetry axis corresponding to the wind direction represented by $\phi = 0$. (We will assume that there are no strong swell components that are not aligned with the wind). Because of the reflection symmetry, it is shown in [Yueh et al., 1993], where the general polarimetric scattering and emission properties of targets with reflection symmetry are presented, that I and Q are even functions of ϕ, whereas U and V are odd functions. Hence, to the second harmonics of ϕ,

$$\begin{aligned} I &\simeq I_0 + I_1 \cos\phi + I_2 \cos 2\phi \\ Q &\simeq Q_0 + Q_1 \cos\phi + Q_2 \cos 2\phi \\ U &\simeq U_1 \sin\phi + U_2 \sin 2\phi \\ V &\simeq V_1 \sin\phi + V_2 \sin 2\phi \end{aligned} \tag{2}$$

When there is no up- and down-wind asymmetry in the surface features, for example, untilted small-scale sea surfaces, the spectral density of the surface is symmetric with respect to the origin, and the Stokes vector can be shown to consist of the following symmetry

$$I_s(\phi) = I_s(\phi + 71) \tag{3}$$

which implies that $I_1 = Q_1 = U_1 = V_1 = 0$. Hence, the Fourier series can be further simplified to

$$\begin{aligned} I &\simeq I_0 + I_2 \cos 2\phi \\ Q &\simeq Q_0 + Q_2 \cos 2\phi \\ U &\simeq U_2 \sin 2\phi \\ V &\simeq V_2 \sin 2\phi \end{aligned} \tag{4}$$

Note that the above relations are derived purely on the symmetry assumption, and are valid for any zenith angle θ, as long as the surface features do not have up- and down-wind asymmetry.

In the following, we discuss how the emissivity of rough surfaces can be related to the bistatic scattering coefficients of the surfaces by the Kirchhoff's law, which was originally derived by Peake [1958] for any polarization for surfaces with a uniform temperature. By a straightforward extension of Peake's argument [Yueh and Kwok, 1992b], the Stokes vector can be expressed in terms of the polarimetric bistatic scattering coefficients. That is the Stokes vector of the thermal emission from the surface plus all the reflected downwelling unpolarized radiation should be unpolarized and with the same specific intensity, when the surface is in thermal equilibrium with the surroundings. Consequently, the Stokes vector of the thermal emission from the surface with the surface temperature T_s is,

$$I_s = I_z - I_r \tag{5}$$

where I_z is the Stokes vector for an unpolarized radiation

$$I_z = T_s \begin{bmatrix} 1 \\ 1 \\ 0 \\ 0 \end{bmatrix} \tag{6}$$

and I_r corresponds to the total reflected radiation by the surfaces for the downwelling radiation. In terms of the polarimetric bistatic scattering coefficients $\gamma_{\alpha\beta\mu\nu}$ (see Appendix I) integrated over all the incident angles in the upper hemisphere, I_r can be expressed as

$$I_r = \int_0^{\pi/2} \sin\theta_i d\theta_i \int_0^{2\pi} d\phi_i \frac{\cos\theta_i}{4\pi\cos\theta} \begin{bmatrix} \gamma_{hhhh}(\theta,\phi;\theta_i,\phi_i) + \gamma_{hvhv}(\theta,\phi;\theta_i,\phi_i) \\ \gamma_{vvvv}(\theta,\phi;\theta_i,\phi_i) + \gamma_{vhvh}(\theta,\phi;\theta_i,\phi_i) \\ 2Re(\gamma_{vhhh}(\theta,\phi;\theta_i,\phi_i) + \gamma_{vvhv}(\theta,\phi;\theta_i,\phi_i)) \\ 2Im(\gamma_{vhhh}(\theta,\phi;\theta_i,\phi_i) + \gamma_{vvhv}(\theta,\phi;\theta_i,\phi_i)) \end{bmatrix} \tag{7}$$

Here, θ and ϕ signify the zenith and azimuth angles of the observation direction.

111. SPM for anisotropic random rough surfaces

This section presents the expression of the Stokes vector derived by using the second-order SPM for surfaces with anisotropic directional spectra. The surface scattering problem

is formulated by the Extended Boundary Condition method, which relates the surface tangential fields to the incident fields. Subsequently, the equations for the surface fields are solved to second order by the perturbation method for small rms height. Here, we summarize the results, and refer the readers to the paper by Yueh et al. [1988] for the detailed formulation and derivation of the SPM.

As the SPM is applied to random rough surfaces, the scattered field can be decomposed into coherent and incoherent components. The zeroth-order scattered field is a coherent field propagating in the specular reflection direction without de-polarization, characterized by the Fresnel reflection coefficients $R_{hh}^{(0)}$ and $R_{vv}^{(0)}$ for horizontal and vertical polarizations, respectively. However, the first-order scattered field is incoherent and contributes to the lowest-order incoherent bistatic scattering coefficients. As the SPM is derived to second order for surfaces with anisotropic directional spectra, we find that the second-order scattered field is coherent and gives a correction to the coherent reflection coefficients of the surfaces. Furthermore, the Cross-Polarized components of the second-order coherent field are not zero when the incident direction is not aligned with the symmetry directions of surfaces.

In conclusion, the modified coherent reflection matrix with the zeroth- and second-order fields considered can be written as

$$R = \begin{bmatrix} R_{hh} & R_{hv} \\ R_{vh} & R_{vv} \end{bmatrix} = \begin{bmatrix} R_{hh}^{(0)} + R_{hh}^{(2)} & R_{hv}^{(2)} \\ R_{vh}^{(2)} & R_{vv}^{(0)} + R_{vv}^{(2)} \end{bmatrix} \tag{8}$$

where $R_{\alpha\beta}^{(2)}$ is the reflected coefficient of 'α' polarized component of the second-order scattered field with 'β' polarized, unit-amplitude incidence, and is related to the spectral density function $W(k_x, k_y)$ by the following integral:

$$R_{\alpha\beta}^{(2)} = \int_{-\infty}^{\infty}\int_{-\infty}^{\infty} dk_x dk_y W(k_{xi} - k_x, k_{yi} - k_y) f_{\alpha\beta}^{(2)} \tag{9}$$

where k_{xi} and k_{yi} are the transverse components of the incident wave vector, and the expression of $f^{(2)}_{\alpha\beta}$ is given in Appendix III.

Additionally, the incoherent polarimetric bistatic scattering coefficients due to the first-order scattered field can be expressed as

$$\gamma^{i}_{\alpha\beta\mu\nu}(\theta,\phi;\theta_i,\phi_i) = \frac{4\pi k_0^2 \cos^2\theta\, \Gamma_{\alpha\beta\mu\nu}(k_x,k_y,k_{xi},k_{yi}) W(k_x - k_{xi}, k_y - k_{yi})}{\cos\theta_i} \tag{10}$$

where k_0 is the free-space wavenumber. θ_i and ϕ_i correspond to the zenith and azimuth angles of the incidence direction, respectively. Likewise, θ and ϕ represent the zenith and azimuth angles of the scattering direction, respectively. The expressions of $\Gamma_{\alpha\beta\mu\nu}$, k_x, k_y, k_{xi} and k_{yi} are given in Appendix II.

Given the above results, I_r can be decomposed into I_{rc} and I_{ri}, the coherent and incoherent reflectivities of surfaces, respectively. That is

$$I_r = I_{rc} + I_{ri} \tag{11}$$

where I_{ri} due to the incoherent bistatic scattering coefficients can be easily obtained from Eq. (7) by replacing $\gamma_{\alpha\beta\mu\nu}$ with $\gamma^{i}_{\alpha\beta\mu\nu}$, and the coherent reflectivity vector, I_{rc}, can be written as

$$I_{rc} = \begin{bmatrix} |R_{hh}|^2 + |R_{hv}|^2 \\ |R_{vv}|^2 + |R_{vh}|^2 \\ 2Re(R_{vh}R^*_{hh} + R_{vv}R^*_{hv}) \\ 2Im(R_{vh}R^*_{hh} + R_{vv}R^*_{hv}) \end{bmatrix} \cdot \begin{vmatrix} |R^{(2)}_{hh}|^2 + |R^{(2)}_{hv}|^2 \\ |R^{(2)}_{vv}|^2 + |R^{(2)}_{vh}|^2 \\ 2Re(R^{(2)}_{vh}R^{(2)*}_{hh} + R^{(2)}_{vv}R^{(2)*}_{hv}) \\ 2Im(R^{(2)}_{vh}R^{(2)*}_{hh} + R^{(2)}_{vv}R^{(2)*}_{hv}) \end{vmatrix} \tag{12}$$

Note that $R^{(2)}_{\alpha\beta}$ and $\gamma^{i}_{\alpha\beta\mu\nu}$ are of the same order because both of them are proportional to the spectral density W. Hence, we remove the square of $R^{(2)}_{\alpha\beta}$ in order to have the terms included only up to the same order of magnitude.

IV. Comparison of the SPM with the Monte Carlo simulation for the emission from 1-D rough surfaces

In order to verify the accuracy of the Stokes vector derived using the second-order SPM for anisotropic random rough surfaces, we carry out a Monte Carlo simulation for the polarimetric emissivities of one-dimensional random rough surfaces with a power-law spectrum.

In simulating the rough surfaces, the surface spectral density function is assumed as follows:

$$W(k_x, k_y) = q \sum_{n=1}^{10} k_x^{-3} \delta(k_x - nk_l)\delta(k_y) \tag{13}$$

where δ is the delta-function, and $k_l = 2\pi/5\lambda$ is the low-wavenumber cutoff. Here λ is the electromagnetic wavelength. Independent random numbers with the Gaussian distribution are generated for the real and imaginary parts of each Fourier component of the surfaces and further weighted by the desired spectral density $k_x^{-3/2}$. The simulated Fourier spectra are then transformed to the spatial domain by the FFT. Each simulated surface is five wavelength long and has 40 samples per wavelength. The surface height between these sampled points is linearly interpolated to create a continuous surface profile. Ten surfaces are generated, and the factor 'q' is adjusted for the desired rms surface height (σ). The surfaces simulated by this approach are periodic with the period corresponding to the low-wavenumber cutoff. To solve the scattering coefficients of all the reflected Floquet modes for both horizontally and vertically polarized incident waves, the Method of Moment with triangular basis for surface tangential fields and pulse weighting is used. Once the scattering coefficients are obtained, the Stokes vectors for the emission from the simulated random surfaces are calculated according to the Kirchhoff's law. Finally, the average of the Stokes vectors of these ten realizations is taken to represent the Stokes vector of the

random surfaces.

Figure 2 illustrates the Stokes parameters as a function of the azimuth angle ϕ for nadir viewing (θ = 0 degrees). The rms surface height is $\lambda/15$, which can be translated into $k_0\sigma$ = 0.419. The dielectric constant of $45 + i30$ is assumed for the surfaces. The results talc.ulatcxl by using the SPM are in close agreement with those obtained from the Monte Carlo simulation. Additionally, it is found that the Stokes parameters have a $\cos 2\phi$ variation in azimuth for T_h and T_v, $\sin 2\phi$ for U, and zero for V, which are expected for nadir viewing (see Section V] for detailed explanation).

Figure 3 presents the results for off-nadir viewing with θ = 50 degrees, while other parameters are the same as those used for Figure 2. Again, excellent agreement is seen between the SPM and the Monte Carlo simulation. Note that in Figure 3 sharp transitions of the Stokes parameters are observed at many azimuth angles. Those are caused by the transition of a particular Floquet mode from radiation to evanescence or vice versa at these angles, which is a special feature of periodic surface scattering [Yueh et al., 1988].

In Figure 4, we plot the Stokes parameters as functions of the zenith angle θ with a fixed azimuth angle ϕ = 45 degrees. The SPM and the Monte Carlo simulation agree very well with each other. For most of θ, the third Stokes parameter, U, is about - 2 degrees Kelvin, and the fourth Stokes parameter, V, remains much smaller than U.

Next, we raise the rms surface height to $\lambda/10$, which is 1.5 times of that used for Figures 2 to 4, and the results are presented in Figures 5 and 6, respectively, for a fixed θ or ϕ. The signatures observed are essentially the same as those seen in Figures 3 and 4, except that the magnitudes of variation are increased by a factor of 2.25 which is expected because the correction terms of the coherent reflection coefficients ($R^{(2)}_{\alpha\beta}$) and the

incoherent bistatic scattering coefficients ($\gamma^i_{\alpha\beta\mu\nu}$) are both proportional to the variance of surface height.

To demonstrate the significance of the corrections introduced by the second-order coherent field, we illustrate the components of the reflectivity vectors, I_r, I_{rc}, and I_{ri}, in Figures 7 and 8 for the results presented in Figure 3 and 4. Note that the magnitudes of incoherent and coherent components of U always increase or decrease together, while carrying a different sign. In particular, the total U is *always* smaller than either one of them. This shows that it is necessary to include the corrections due to the second-order coherent field in the calculation of the Stokes vector. Otherwise, significant errors are expected in the magnitude and the signs of the third Stokes parameter.

v. Emission from Small-scale sea surfaces

This section presents the results of the application of the SPM to the untilted small-scale sea surfaces. Although the tilting effects of the large-scale surface variation and other sea surface features, such as foams, are not considered, we do not expect that the directional signatures of the Stokes vector predicted here deviate significantly from those with these features considered.

The small-scale wind-induced surfaces are described by an empirical surface spectrum, which was proposed by Durden and Vesecky [1985], and was shown to be able to explain the sea surface backscattering from many aircraft measurements. Due to some typographical errors found in their paper, the correct expressions of these formulas are included in Appendix IV. The spectrum of the small-scale surface is set to be the same as that of the complete spectrum for the wavenumbers above a certain cutoff, and set to be zero,

otherwise. This is a typical approach used by two scale sea surface scattering models. The cutoff wavenumber is selected in such a way that $k_0\sigma$ equals to a value of 0.25. Other cutoff selections ($k_0\sigma$ between 0.2 and 0.3) have also be studied, and the signatures remain similar to those of $k_0\sigma = 0.25$. Note that the cutoff wavenumber actually differs from one wind speed to another because we hold $k_0\sigma$ as a constant for the spectra of all wind speeds. Though this may not be the best way to select the wavenumber cutoff, we expect that the values calculated from this cutoff selection give a useful indication of the signatures of sea surface emissions. In addition, the accuracy of the SPM can be ensured because the value 0.25 is smaller than the values used in the previous section for the verification of the SPM. The surface spectrum parameters reported in [Durden and Vesecky, 1985] are used in this paper except the parameter a_0, which is increased to 0.008 from 0.004 of Durden and Vesecky in order to have the magnitude of the peak-to peak variation of T_h and T_v over azimuth angles agreed with those reported by Etkin et al. [1991] and Wentz [1992], and the values of U comparable to those shown in [Mizura et al., 1992]. It is believed that part of this discrepancy in spectral amplitude is due to the uncertainty of the sea spectra at high wavenumbers, which are not yet well understood, and part of that is due to the sea surface features which are not accounted for in this paper.

Figure 9 illustrates the Stokes parameters as functions of the azimuth angle for four wind speeds for nadir viewing at $f = 19.3$ GHz. It can be seen that the directional features of the Stokes parameters are just like those of one-dimensional surfaces presented in the previous section, and the magnitude of the azimuthal variation increases as the wind speed increases.

In Figures 10 and 11, we illustrate the Fourier expansion coefficients of Stokes parameters as functions of wind speeds at various zenith angles with the surface parameters the

same as those used for Figure 9. Figures 10(a) shows that for all zenith angles, I_0 is a monotonically increasing function of wind speed. However, as shown in Figure 10(b), Q_0 is fairly insensitive to the wind speed at near nadir viewing ($\theta \leq 20$). This suggests that the Stokes parameter I is a better indicator of the wind speed than the parameter Q.

Figure 11 illustrates the coefficients of the second harmonics as functions of wind speeds. As expected, the magnitudes of Q_2 and U_2 increase as the wind speed increases, because of the increase in surface roughness at higher wind speeds. Furthermore, I_2 is zero at $\theta = 0$ degree, and deviates from zero as θ increases, indicating that the parameter I is insensitive to the wind direction at near nadir angles. Another interesting feature is that Q_2 is approximately equal to the negative of U_2 for θ smaller than 20 degrees. This relation will be shown to be exact for $\theta = 0$ degree in the next section and explains the azimuthal signatures illustrated in Figure 5 in [Dzura et al., 1992].

In the results presented above, it can be noticed that the wind speed sensitivities of all the Stokes parameters decrease as the observation angle θ increases. This is consistent with the brightness temperatures, T_h and T_v, of sea surfaces measured from aircrafts [Sasaki et al., 1987], and can be explained by the nature of the SPM which assumes a small parameter $\xi = k_0\sigma\cos\theta$ for perturbation expansion. Because the factor $\cos\theta$ reaches maximum at $\theta = 0$ (or normal incidence), the surfaces will appear to be rougher electromagnetically (larger ξ) at near normal incidence than at large incidence angles. Consequently, the reflectivities (or emissivities) of the surfaces are more sensitive to the small-scale surface perturbations at near normal incidence than large incidence angles.

In summary, the theoretical values of Stokes parameters near nadir angles for small-

scale sea surfaces can be approximated as:

$$
\begin{aligned}
I &\simeq a_i + g(U_{19.5}) \\
Q - Q0 &= h(U_{19.5})\cos 2\phi \\
U &= h(U_{19.5})\sin 2\phi \\
V &\simeq 0
\end{aligned}
\tag{14}
$$

Here, g is a monotonic increasing function (approximately linear) of the wind speed at 19.5 meters ($U_{19.5}$), which is consistent with the aircraft-measured wind speed dependence [Sasaki, 1987]. In addition, h is also a quasi-linear function of $U_{19.5}$ according to the theoretical results presented in Figure 11. Nevertheless, since the tilting effects of the large scale surface together with other surface features have not been considered, and since the wavenumber cutoff may not be appropriate for all wind speeds, h is likely to be a more complicated function of wind speed for actual sea surfaces.

VI. Single-look polarimetric radiometry for wind vector retrieval

This section discusses the application of polarimetric radiometry to ocean wind vector retrieval and how the polarimetric information can be used to reduce the number of azimuth looks for spaceborne sensor designs.

Here, we discuss the cases of near nadir viewing because of the very simple form of the model functions described by Equations (4) or (14), which allows an easier explanation of concept. Nevertheless, it is expected that the idea is also applicable to larger incidence angles, though the general form of model function given by Eq. (2), which implies a more complicated inversion procedure, has to be considered.

In the following, we derive the functional form of the Stokes parameters at the nadir

angle by using the antenna coordinate rotation. Specifically, we will show that at nadir viewing, the Stokes parameters at any azimuth angles are completely characterized by the brightness temperatures of horizontal and vertical polarizations (T_{h0} and T_{v0}) at $\phi = 0$. Let us assume that the vertical polarization of the antenna at $\phi = 0$ be parallel to the wind direction, and at an angle ϕ, the vertical polarization makes an angle of ϕ and $\pi/2 - \phi$, respectively, with the vertical and horizontal polarization channels at $\phi = 0$. Therefore the horizontally and vertically polarized electric fields at any ϕ can be transformed from those (E_{h0} and E_{v0}) at $\phi = 0$ by the rotation transformation:

$$\begin{aligned} E_v(\phi) &= E_{v0}\cos\phi + E_{h0}\sin\phi \\ E_h(\phi) &= -E_{v0}\sin\phi + E_{h0}\cos\phi \end{aligned} \tag{15}$$

From the definition of Stokes parameters, it can be easily shown that the Stokes parameters at any ϕ are related to T_{h0} and T_{v0} by:

$$\begin{aligned} I(\phi) &= T_{v0} + T_{h0} \\ Q(\phi) &= (T_{v0} - T_{h0})\cos 2\phi \\ U(\phi) &= -(T_{v0} - T_{h0})\sin 2\phi \\ V(\phi) &= 0 \end{aligned} \tag{16}$$

where the fact that both U and V are zeros at $\phi = 0$ have been used in the derivation.

The above relations derived at the nadir angle show that the Stokes parameters Q and U have a $\cos 2\phi$ and a $\sin 2\phi$ variations, respectively, and I is not a function of ϕ. In addition, Eq. (16) confirms the form of model function shown in Eq. (14) inferred from theoretical data.

Hence, given the values of Q and U at near nadir angles, we obtain the following equation for ϕ

$$\tan 2\phi = -\frac{U}{Q - Q_0} \tag{17}$$

from Eq. (14). Note that the above equation provides four solutions for ϕ forming a rectangular cross within a 360-degree azimuth span. However, two of them can be eliminated by inspecting the sign of U, while the remaining two differ from each other by 180 degrees. This shows that the streamline of the wind field can be uniquely defined with a single-look configuration by measuring the first three Stokes parameters at near nadir angles.

Besides the wind direction, the wind speed can be retrieved with various methods: For example,

$$U_{19.5} = h^{-1}(\sqrt{(Q - Q_0)^2 + U^2}) \tag{18}$$

or

$$U_{19.5} = g^{-1}(I - a_i) \tag{19}$$

Note that both equations do not require the information of wind direction. However, the applicability of the Eq. (18) depends on the invertibility of the function h and also on the wind speed sensitivity of h, while the use of the parameter I for wind speed inversion is expected to be straightforward because of its monotonic dependence on wind speed, indicated in the aircraft measurements [Sasaki, 1987] and the results shown in Figure 10(a). The tradeoff for inverting the wind speed is that the parameter I is more susceptible to atmospheric noises, while allowing an easy implementation of wind speed inversion. In contrast, though Q and U are less susceptible to atmospheric noises, the wind speed dependence of these requires further investigation.

Besides the above inversion scheme which treats I independently of Q and U, the first three Stokes parameters can be used together to estimate the value of wind speed by minimizing the mean square difference of measurements and model function. However, the optimum scheme shall depend on the actual form of the model function.

From the above discussion, we conclude that a single-look polarimetric radiometer is viable in retrieving the wind vectors with two ambiguous directions with 180° apart for θ ranging from nadir to an angle of up to 20 or 30 degrees.

For the cases of off-nadir viewing, the general form of the model function shown in Eq. (2) has to be taken into consideration, due to the fact that the odd-harmonics in the Fourier expansion of the Stokes parameters are not expected to be negligible as indicated by the SSM/I data ($\theta = 53°$) [Wentz,1992]. This increases the complexity of wind vector inversion because the equations for wind direction and speed are no longer decoupled. However, this up- and down-wind asymmetry may actually lead to the unique determination of wind direction, unlike the cases of near nadir angles, where two ambiguities with a 180-degree difference can not be resolved without, additional information.

VII. Summary and Discussions

In this paper, a second-order SPM is presented to analyze the polarimetric emission from two-dimensional random rough surfaces with an anisotropic directional spectrum. The accuracy of the SPM calculations was quantified by the Monte Carlo simulation technique for the emission from one-dimensional rough surfaces with a power law spectrum. Subsequently, we apply the SPM to the small-scale sea surfaces, and derive the model function of the Stokes parameters of sea surface emission.

Additionally, we propose a single-look polarimetric radiometer for wind vector retrieval. The procedure of inversion is discussed in details for the cases of near nadir angles, and is shown to be straightforward for implementation. For the cases of off-nadir observations, we expect that the wind direction can be uniquely determined because of the up-

and down-wind asymmetry in the model function, though the method of inversion will not be as straightforward as the cases of near nadir angles.

The results of this paper indicate that the passive polarimetry is a promising technique for the remote sensing of ocean wind vector. However, several issues not addressed in this paper need further investigation by either more extended theoretical analyses or measurements to determine the model function of Stokes parameters. In this regard, experiments should be carried out for sea surface emission at a large range of observation angles θ from 0 up to 60 degrees, which are important for spaceborne remote sensing applications. In addition, theoretical analysis should be extended to account for the tilting effects of large scale surfaces and other sea surfaces features, such as foams. Another issue is the selection of the operational frequency band of the radiometer measurements for ocean wind field applications. In other words, the sensitivity of wind speed and direction versus the microwave frequency should be determined. Finally, the design of a polarimetric radiometer which is capable of measuring at least the first three Stokes parameters with the required accuracy and stability should be studied.

Acknowledgment

This work was performed under contract with the National Aeronautics and Space Administration at the Jet Propulsion Laboratory, California Institute of Technology. The authors would like to thank S. Durdean and Y. Kim for many valuable discussions and information.

Appendix 1. Polarimetric bistatic scattering coefficients

Let us introduce a polarimetric scattering matrix element $f_{\alpha\beta}(\theta, \phi; \theta_i, \phi_i)$ to describe the scattering from a surface illuminated by a unit-amplitude plane wave with the polarization β from the direction (θ_i, ϕ_i). The polarization component α of the scattered field propagating in the direction (θ, ϕ) can be written as

$$E_\alpha = \frac{\exp(ik_0 r)}{r} f_{\alpha\beta}(\theta, \phi; \theta_i, \phi_i)$$

where r is the range from the receiver to the scattering target, and k_0 is the free space wavenumber.

Given that, the polarimetric bistatic scattering coefficients can be defined as

$$\gamma_{\alpha\beta\mu\nu}(\theta, \phi; \theta_i, \phi_i) = \frac{4\pi}{A \cos\theta_i} < f_{\alpha\beta}(\theta, \phi; \theta_i, \phi_i) f^*_{\mu\nu}(\theta, \phi; \theta_i, \phi_i) >$$

where A is the illuminated area.

Appendix 11. First-order scattering coefficients

The coefficients for the incoherent bistatic scattering coefficients due to the first-order scattered fields are defined as:

$$\Gamma_{\alpha\beta\mu\nu}(k_x, k_y, k_{xi}, k_{yi}) = f^{(1)}_{\alpha\beta}(\theta, \phi; \theta_i, \phi_i) f^{(1)*}_{\mu\nu}(\theta, \phi; \theta_i, \phi_i)$$

with

$$f^{(1)}_{hh}(\theta, \phi; \theta_i, \phi_i) = \frac{2k_{zi}(k_1^2 - k_0^2)}{k_z + k_{1z}} \frac{1}{k_{zi} + k_{1zi}} \left(\frac{k_{xi} k_x}{k_{\rho i} k_\rho} + \frac{k_{yi} k_y}{k_{\rho i} k_\rho} \right)$$

$$f^{(1)}_{hv}(\theta, \phi; \theta_i, \phi_i) = \frac{2k_{zi}(k_1^2 - k_0^2)}{k_z + k_{1z}} \frac{k_{1zi} k_0}{k_1^2 k_{zi} + k_0^2 k_{1zi}} \left(- \frac{k_{yi} k_x}{k_{\rho i} k_\rho} + \frac{k_{xi} k_y}{k_{\rho i} k_\rho} \right)$$

$$f^{(1)}_{vh}(\theta, \phi; \theta_i, \phi_i) = \frac{2k_{zi}(k_1^2 - k_0^2)}{k_1^2 k_z + k_0^2 k_{1z}} \frac{k_{1z} k_0}{k_{zi} + k_{1zi}} \left(- \frac{k_{yi} k_x}{k_{\rho i} k_\rho} + \frac{k_{xi} k_y}{k_{\rho i} k_\rho} \right)$$

$$f^{(1)}_{vv}(\theta, \phi; \theta_i, \phi_i) = \frac{2k_{zi}(k_1^2 - k_0^2)}{k_1^2 k_z + k_0^2 k_{1z}} \frac{1}{k_1^2 k_{zi} + k_0^2 k_{1zi}} \left[k_1^2 k_\rho k_{\rho i} - k_0^2 k_{1z} k_{1zi} \left(\frac{k_{xi} k_x}{k_{\rho i} k_\rho} + \frac{k_{yi} k_y}{k_{\rho i} k_\rho} \right) \right]$$

where

$$k_{\rho i} = k_0 \sin\theta_i$$

$$k_{xi} = k_{\rho i}\cos\phi_i$$

$$k_{yi} = k_{\rho i}\sin\phi_i$$

$$k_{zi} = \sqrt{k_0^2 - k_{\rho i}^2}$$

$$k_{1zi} = \sqrt{k_1^2 - k_{\rho i}^2}$$

$$k_\rho = k_0 \sin\theta$$

$$k_x = k_\rho \cos\phi$$

$$k_y = k_\rho \sin\phi$$

$$k_z = \sqrt{k_0^2 - k_\rho^2}$$

$$k_{1z} = \sqrt{k_1^2 - k_\rho^2}$$

and k_0 and k_1 are the electromagnetic wavenumbers of the free space and lower half-space.

Appendix III. Second-order scattering coefficients

The correction terms of the coherent reflection matrix due to the second-order scattered field are given as follows:

$$f_{hh}^{(2)} = \frac{k_1^2 - k_0^2}{k_{zi} + k_{1zi}} \frac{2k_{zi}}{k_{zi} + k_{1zi}} \left\{ k_{1zi} + \frac{(k_0^2 - k_1^2)}{(k_\rho^2 + k_{1z}k_z)(k_z + k_{1z})} \left[k_{1z}k_z + k_\rho^2 \left(\frac{k_{xi}}{k_{\rho i}}\frac{k_x}{k_\rho} + \frac{k_{yi}}{k_{\rho i}}\frac{k_y}{k_\rho} \right)^2 \right] \right\}$$

$$f_{vh}^{(2)} = \frac{k_1^2 - k_0^2}{k_{zi} + k_{1zi}} \frac{2k_0 k_{zi}}{k_1^2 k_{zi} + k_0^2 k_{1zi}} \left(\frac{k_{xi}}{k_{\rho i}}\frac{k_y}{k_\rho} - \frac{k_{yi}}{k_{\rho i}}\frac{k_x}{k_\rho} \right) \left[\frac{k_\rho k_{\rho i} k_1^2}{k_\rho^2 + k_{1z}k_z} + \frac{k_{1zi}k_\rho^2(k_0^2 - k_1^2)}{(k_\rho^2 + k_{1z}k_z)(k_z + k_{1z})} \left(\frac{k_{xi}}{k_{\rho i}}\frac{k_x}{k_\rho} + \frac{k_{yi}}{k_{\rho i}}\frac{k_y}{k_\rho} \right) \right]$$

$$f_{hv}^{(2)} = -f_{vh}^{(2)}$$

$$f_{vv}^{(2)} = \frac{k_0^2 - k_1^2}{k_1^2 k_{zi} + k_0^2 k_{1zi}} \frac{2k_{zi}k_1^2 k_0^2}{k_1^2 k_{zi} + k_0^2 k_{1zi}} \left\{ \frac{k_{\rho i}^2 k_\rho^2 (k_1^2 - k_0^2)}{k_0^2 (k_\rho^2 + k_{1z}k_z)(k_z + k_{1z})} \right.$$

$$+ k_{1zi}\left[1 - \frac{2k_{\rho i}k_\rho}{k_{1z}k_z + k_\rho^2}\left(\frac{k_{xi}}{k_{\rho i}}\frac{k_x}{k_\rho} + \frac{k_{yi}}{k_{\rho i}}\frac{k_y}{k_\rho}\right)\right]$$
$$+ \frac{k_{1zi}^2(k_0^2 - k_1^2)}{k_1^2(k_z + k_{1z})}\left[1 - \frac{k_\rho^2}{k_{1z}k_z + k_\rho^2}\left(\frac{k_{xi}}{k_{\rho i}}\frac{k_x}{k_\rho} + \frac{k_{yi}}{k_{\rho i}}\frac{k_y}{k_\rho}\right)^2\right]\Bigg\}$$

where k_{xi}, k_{yi}, $k_{\rho i}$, k_{zi}, k_{1zi}, k_ρ, k_z, and k_{1z} are the same as those defined in Appendix II.

Appendix IV. Empirical sea surface spectrum

The surface spectrum proposed by Durden and Vesecky [1985] for $k > k_j = 2$ is given as

$$W(k,\phi) = \frac{1}{2\pi k}S(k)\Phi(k,\phi)$$

where

$$S(k) = a_0 k^{-3}\left(\frac{bku_*^2}{g_*}\right)^{a\log_{10}(k/k_j)}$$
$$\Phi(k,\phi) = 1 + c(1 - e^{-sk^2})\cos 2\phi$$

Here, $g_* = g + \gamma k^2$ with $\gamma = 7.25 \times 10^{-5}$ and $g = 9.81$.

The wind speed given at any elevation z can be calculated from u_* by

$$U(z) = \frac{u_*}{0.4}\log\left(\frac{z}{Z_0}\right)$$

where u_* is related to Z_0 by

$$Z_0 = 0.0000684u_* + 0.004287u_*^2 - 0.000443$$

The coefficients of the angular part of the spectrum are

$$c = \left(\frac{1 - R}{1 + R}\right)^2/(1 - D)$$

where

$$R = 0.003 + 0.00192U(12.5)$$
$$D = \frac{\int_0^\infty k^2 S(k)e^{-sk^2}dk}{\int_0^\infty k^2 S(k)dk}$$

Misprints are found in the equations for Z_0, c, and R in the paper by Durden and Vesecky [1985].

References

Ihll'dell, s. 1'., and J. F. Vesecky, "A physical radar cross-section model for a wind driven sea with swell ,') *IEEE J. Oceanic Eng.*, **vol.** OE-10, No. 4, 445-451, 1985.

Dzura, M.S., V. S. Etkin, A. S. Khrupin, M. N. Pospelov, and M. D. Raev, "Radiometers-Polarimeters: principles of design and applications for sea surface microwave emission polarimetry," International Geoscience and Remote Sensing Symposium, Houston, 1992.

Etkin, V. S., M. D. Raev, M. G. Bulatov, Yu. A. Militsky, A.V. Smirnov, V.Yu. Raizer, Yu. A. Trokhimovsky, V.G. Irisov, A.V. Kuzmin, K.Ts. Litovchenko, E.A. Bespalova, E.I. Skvortsov, M. N. P ospelov, and A .1. Smirnov, *Radiohydrophysical A erospace Research of Ocean*, Report Hp-1749, Academy of Sciences, 11 SSR, Space Research Institute, 1991.

Johnson, J. T., J. A. K ong, R. 'J'. Shin, D. H. Staelin, K. O'Neill and A. W. Lohanick, "Third stokes parameter emission from a periodic water surf ace," submitted to *IEEE Trans. Geosci. Remote Sensing*, Oct, 1992.

Johnson, J. 'J'., J. A. Kong, R. 'J'. Shin, S. 11. Yueh, S. V. Nghiem, and R. Kwok, " A numerical analysis of polarimetric thern nal emission from rough ocean surfaces," submitted to J. Electromagnetic Waves and Appl., 1993.

Klein, L.A. and C. T. Swift, "An improved model for the dielectric constant of sea water at microwave frequencies," *IEEE Trans. Ant. and Prop.* Vol. AP-25, 104-111, 1977.

Nghiem, S. V., M. E. Veysoglu, R. 'J'. Shin, J. A. Kong, K. O 'Neill, and A. Lohanick, "] 'olarimetric passive remote sensing of a periodic soil surface: microwave measurements and analysis" J. Electromagnetic Waves and Appl., Vol. 5, No. 9, 997-1005, 1991.

I'cake!, W. }1., "Interaction of electromagnetic waves with some natural surfaces," *IEEE Trans. A nt. and Prop.* Vol. AP-7, S]) CC. S11])])]. 8324-8329, 1959.

Sasaki, Yasunori, Ichio Asanuma, Kei Muneyama, Gen'Ichi Naito, and Tsutomu Suzuki, "The dependence of sea-surface microwave emission on wind speed, frequency, incidence angle, a ı d polarization over the freque ı cy range from 1 to 4 0 GHz," *IEEE Trans. Geosci. and Remote Sensing*, Vol. GE-25, No. 2, 138-146, March, *1987*.

Tsang, 1,., "Polarimetric passive remote sensing of random discrete scatterers and rough surfaces," J. Electromagnetic Waves and Appl., Vol. 5, No, 1, 41-57, 1991.

Tsang, L, J. A. Kong, and R. T. Shin, Theory of Microwave Remote Sensing, Wil - interscience, New York, 1985.

Veysoglu, M. E., S. H. Yueh, R. T. Shin, and J. A. Kong, "Polarimetric passive remote sensing of periodic sm'fac.es, " J. Electromagnetic Waves and Appl., Vol. 5, No. 3, 267-280, 1991.

Wentz, Frank J., "Measurement of oceanic wind vector using satellite microwave radiometers," *IEEE Trans. Geosci. Remote Sensing*, Sept, 1 992.

Yueh, S. H. and R. Kwok, "Polarimetric passive remote sensing of terrain surfaces," International Geoscience and Remote Sensing Symposium, URSI Digest, p. 14, Houston, 1992a.

Yueh, S. H., and R. Kwok, "Electromagnetic fluctuations for anisotropic media and the generalized Kirchhoff's law," accepted for publication in Radio Science, 1 992b.

Yueh, S. **11.,** R. **T.** Shin, and J. A. Kong, "Se.attering of electromagnetic waves from a periodic Sul'face with random roughness," *J. Appl. Phys.*, 64(4), 1 657-1670, 1988.

Yueh, S. H., S. V. Nghiem, R. Kwok, W. J. Wilson, F. 1{. Li, J. '1'. Johnson, and J. A. Kong, "Polarimetric thermal emission from periodic water surf aces," submitted t o *Radio Science*, Dec. 1992.

Yueh, s. 11., et al., "Polarimetric scattering and emission properties of targets with reflection symmetry," paper in preparation, 1993.

Wu, S. T., and A. K. Fung, "A noncoherent model for microwave emissions and backscattering from the sea surf ace," *J. Geophy. Res.*, Vol. 77, No. 30, 5917-5929, 1972.

List of Figures

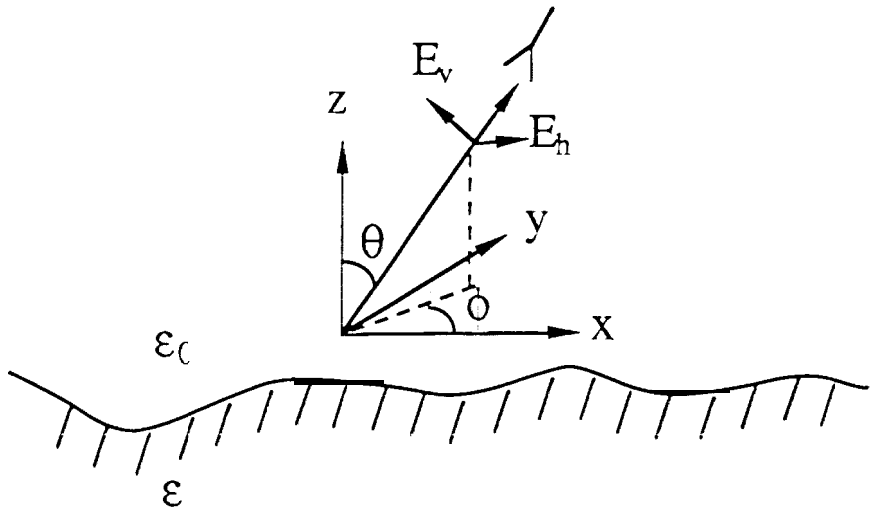
E_v
z
E_h
θ
y
φ
x
ε0
ε

((l)

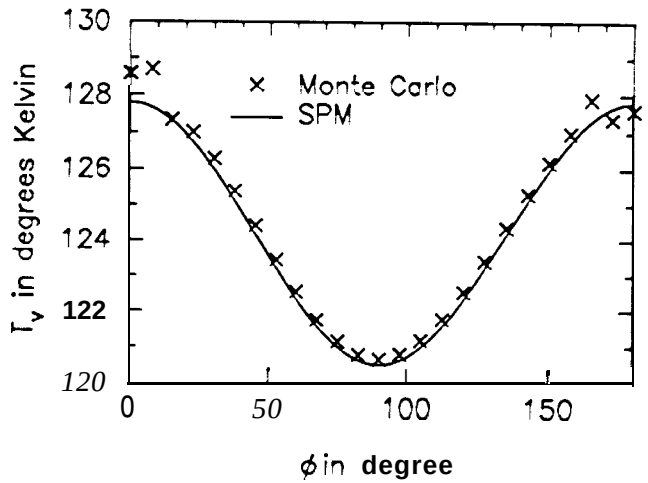

(b)

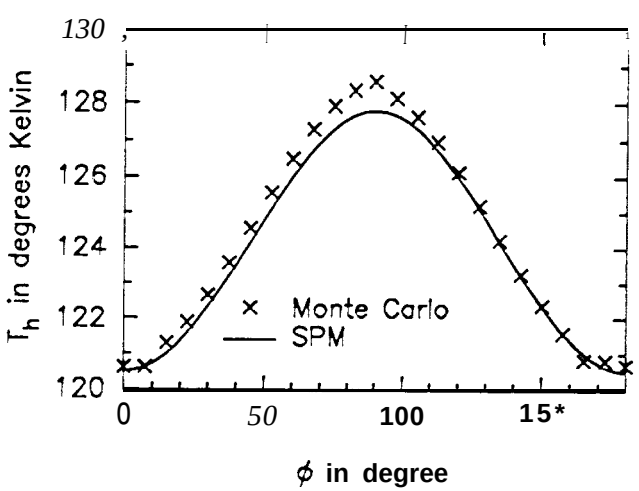

(c)

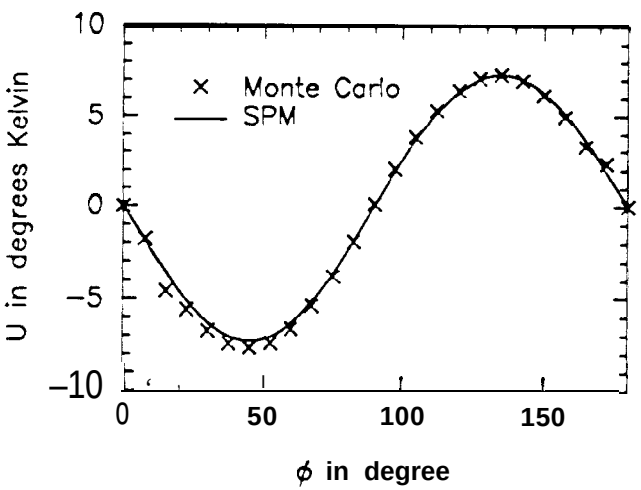

(d)

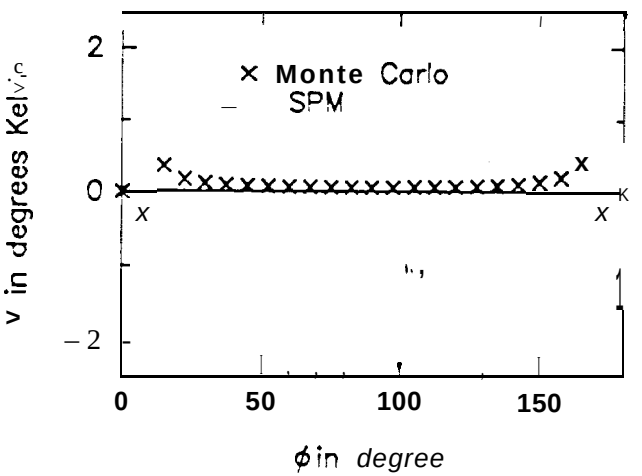

elmon 15-Feb-1993 12:11

Fig. 2

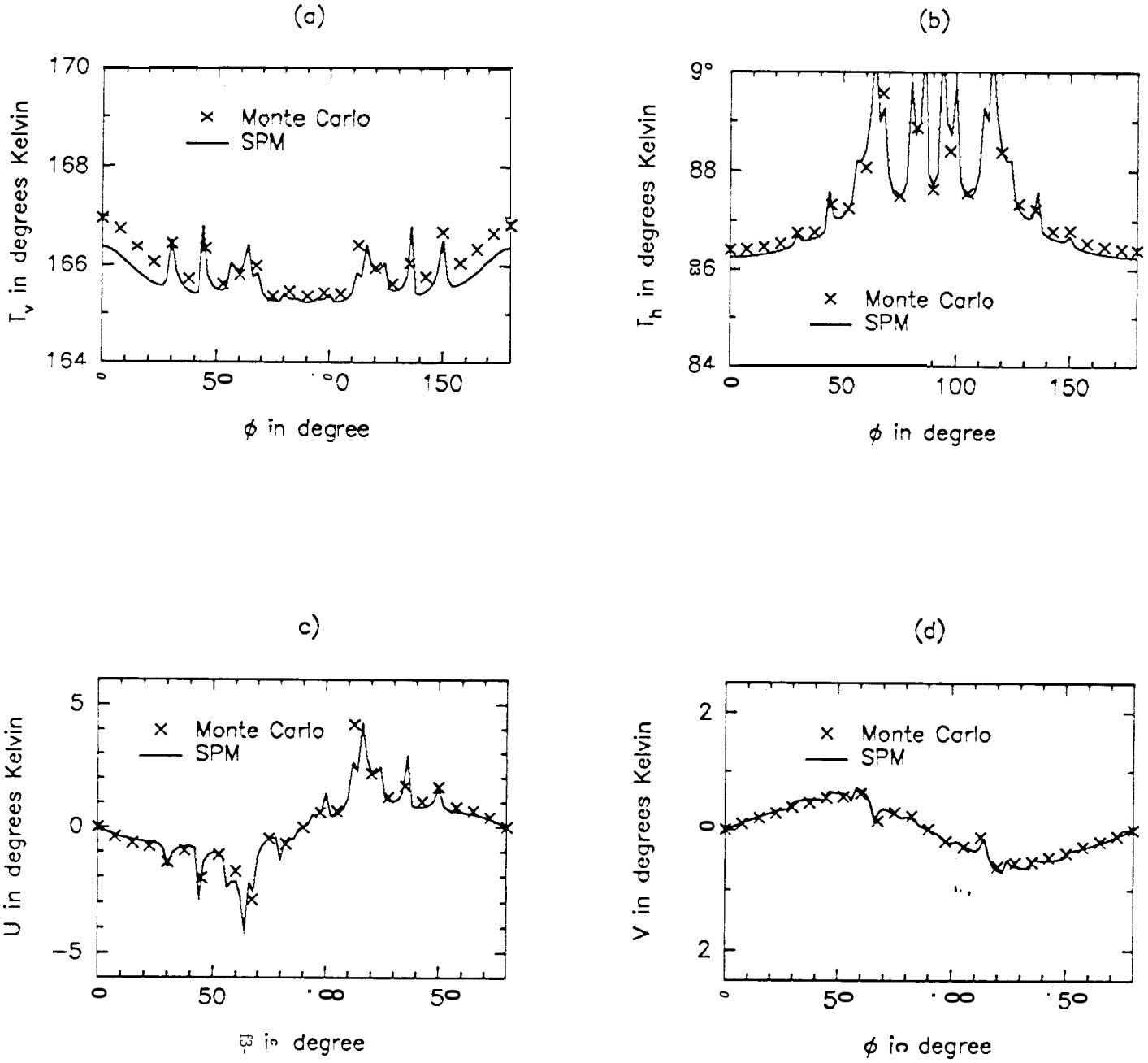

simon 15-Feb-1993 13:58

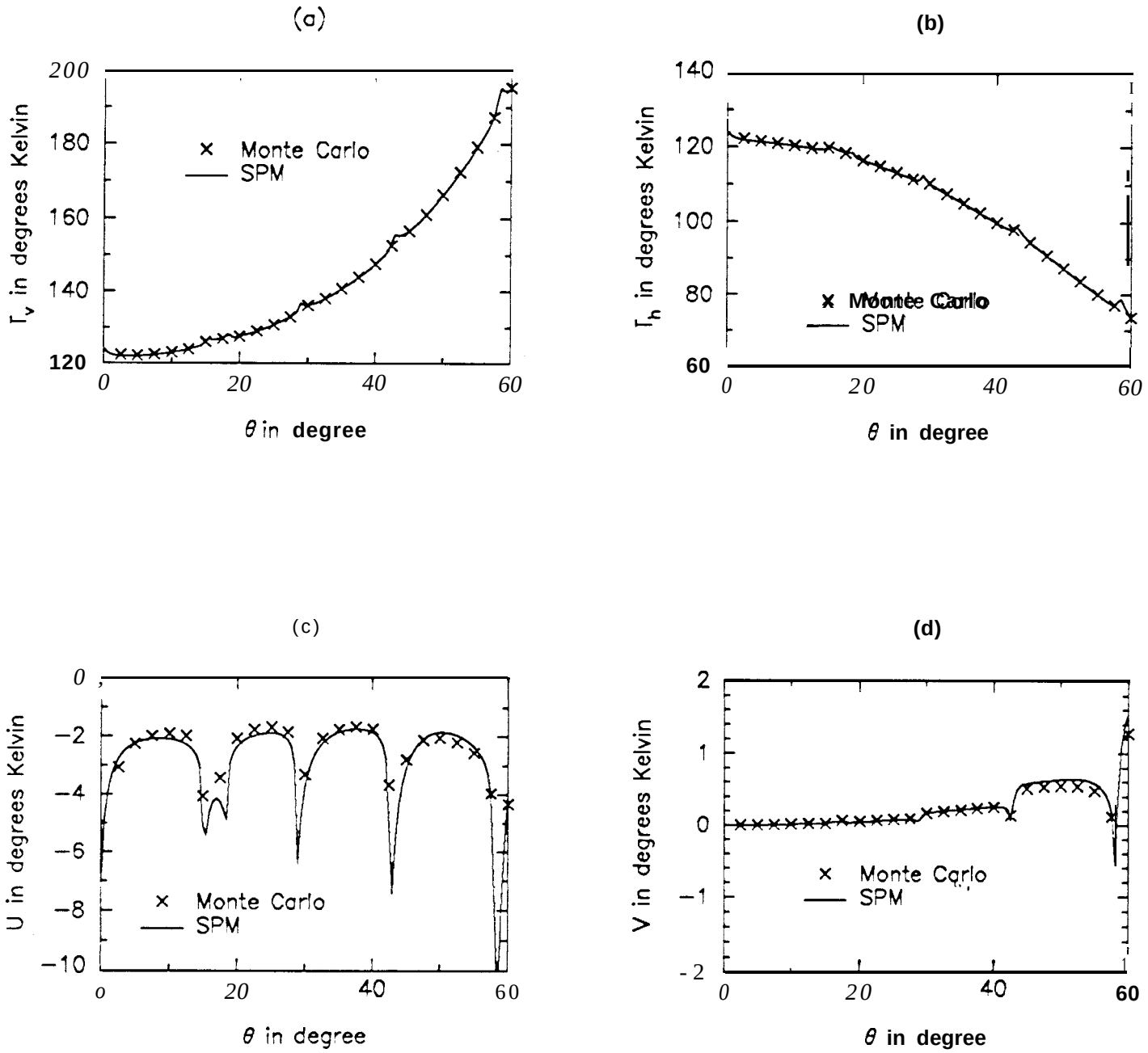

elmon 15-Feb-1993 14:31

Fig.4

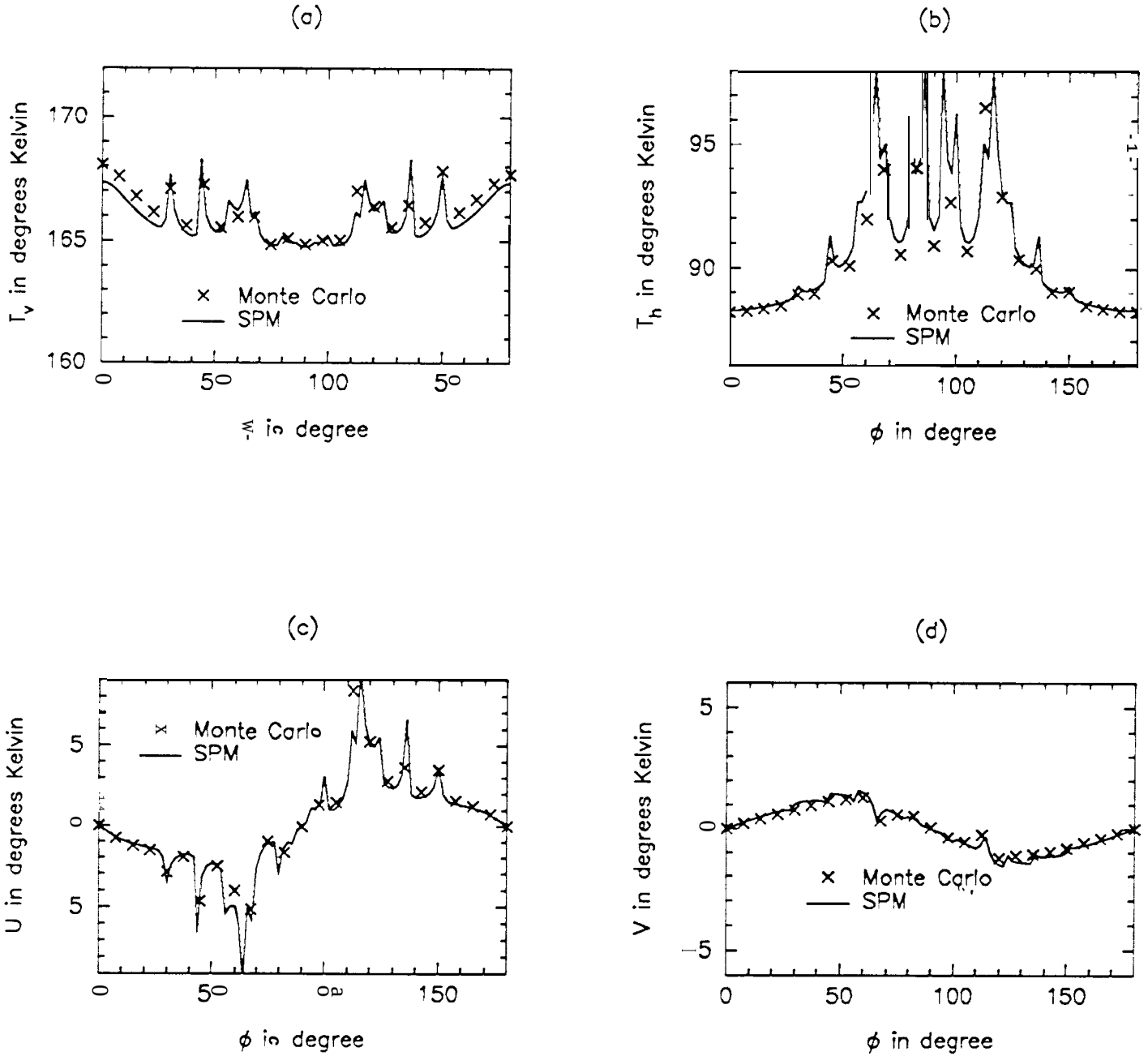

simon 15-Feb-1993 14:09

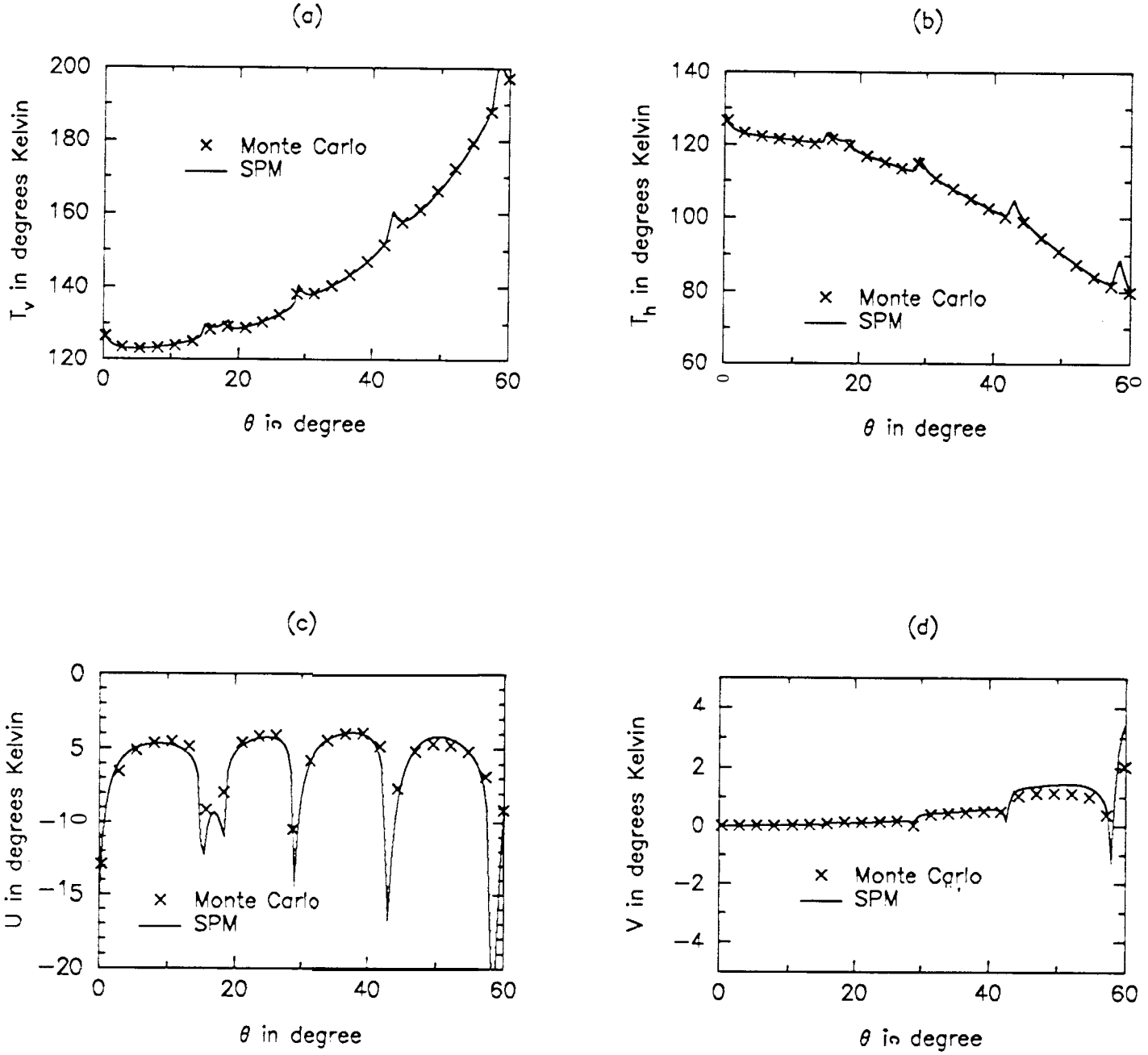

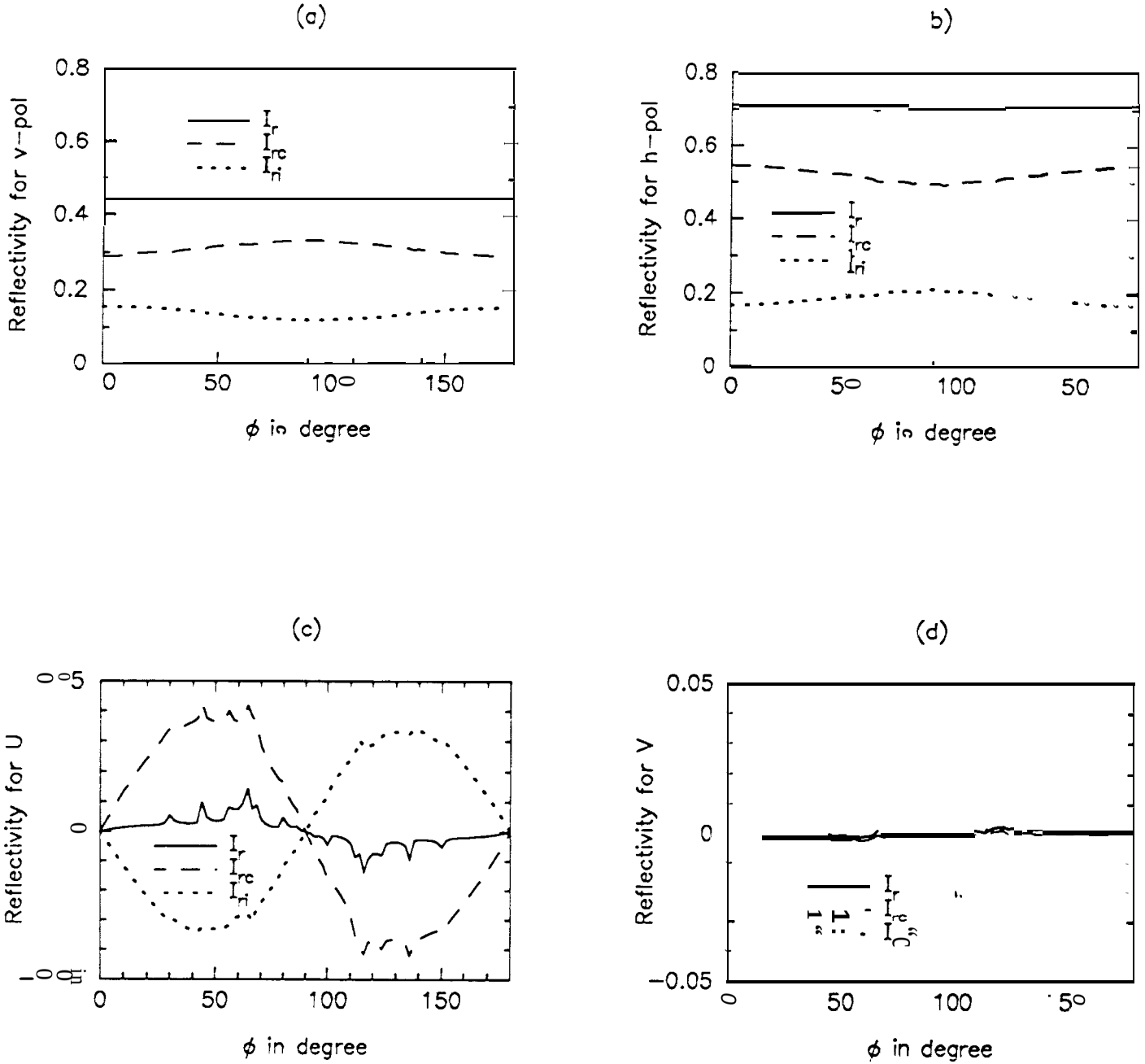

simon 15-Feb-1993 17:38

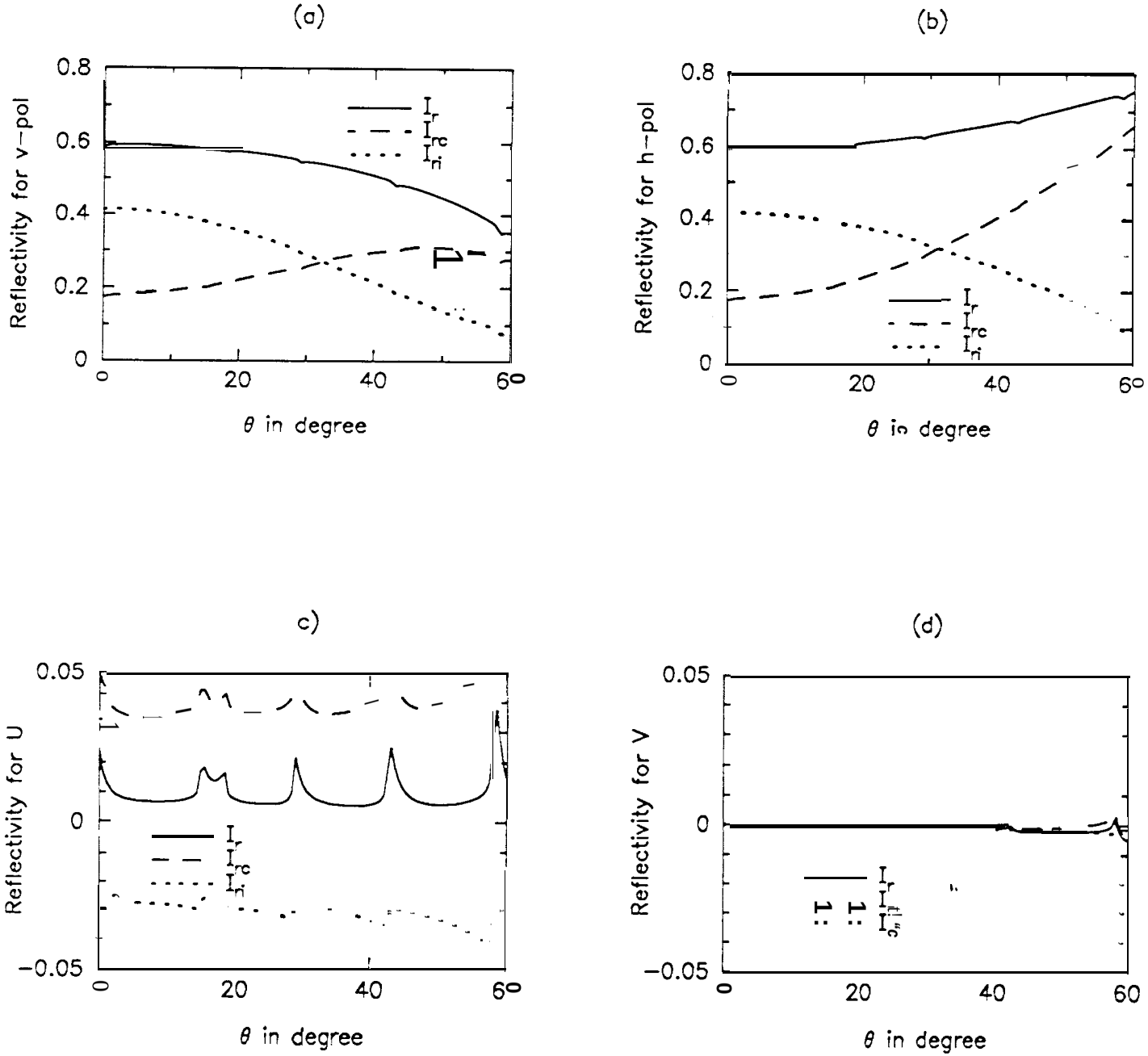

(a)

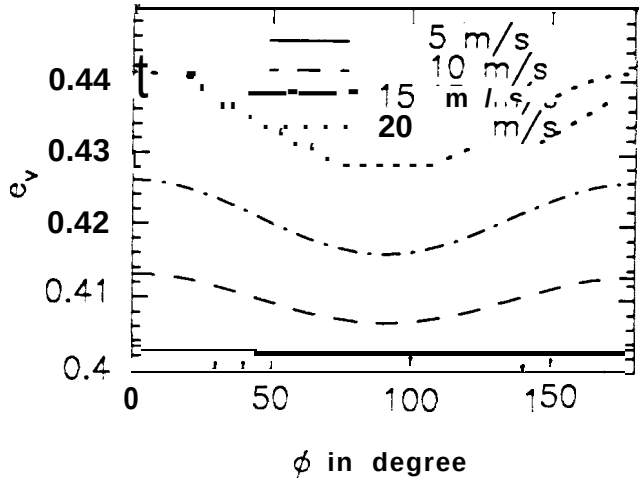

(b)

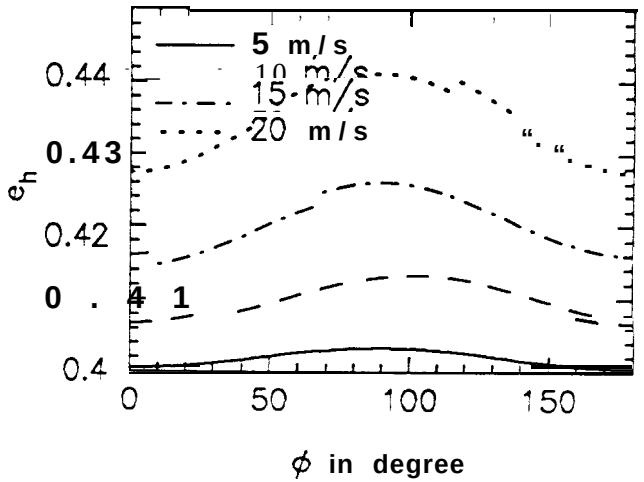

(c)

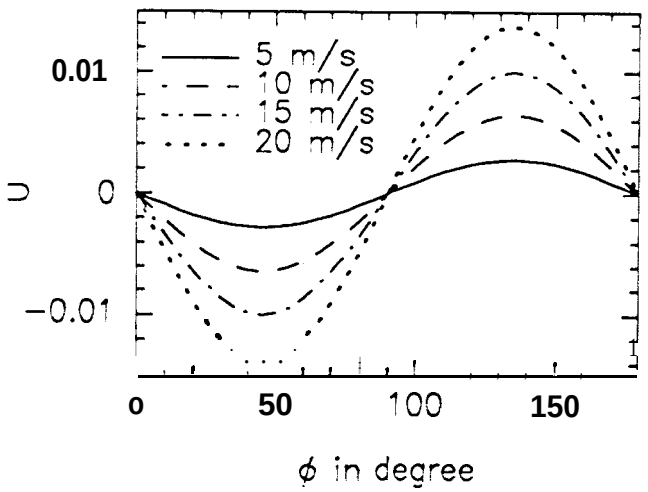

(d)

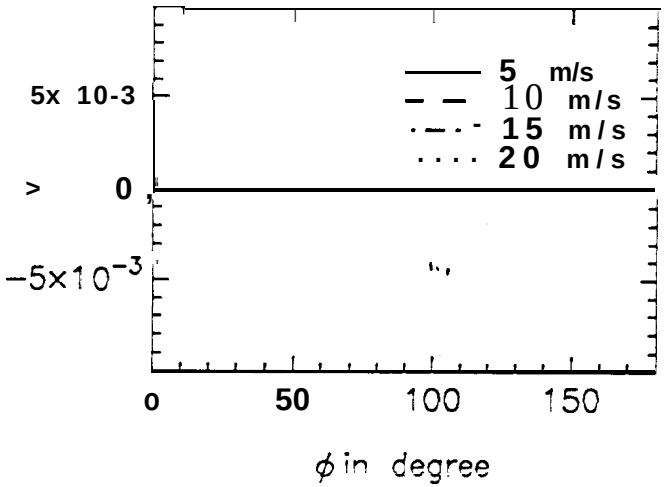

simon 27-Jan-1993 10:38

Fig. 9

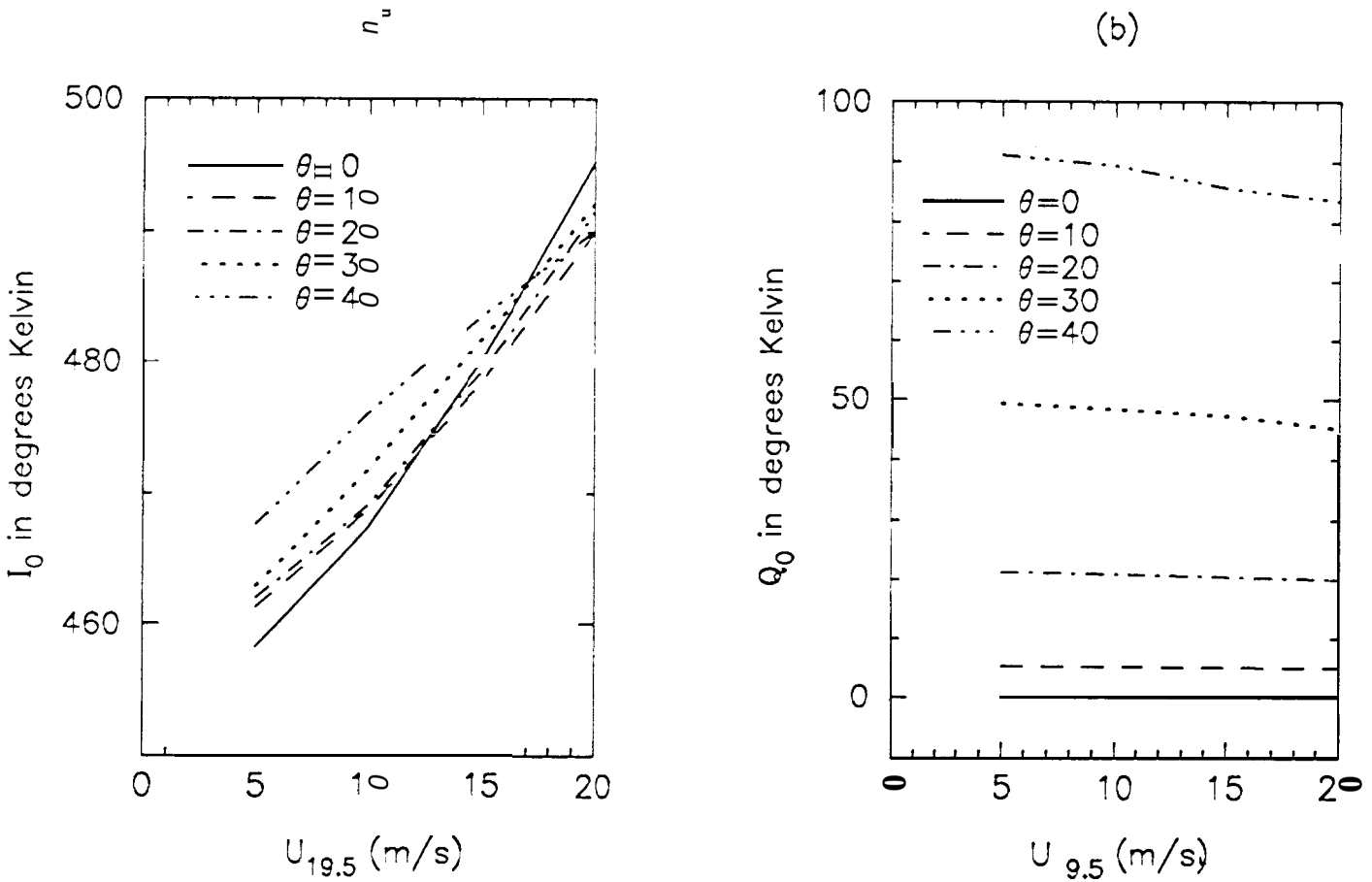

Fig 0

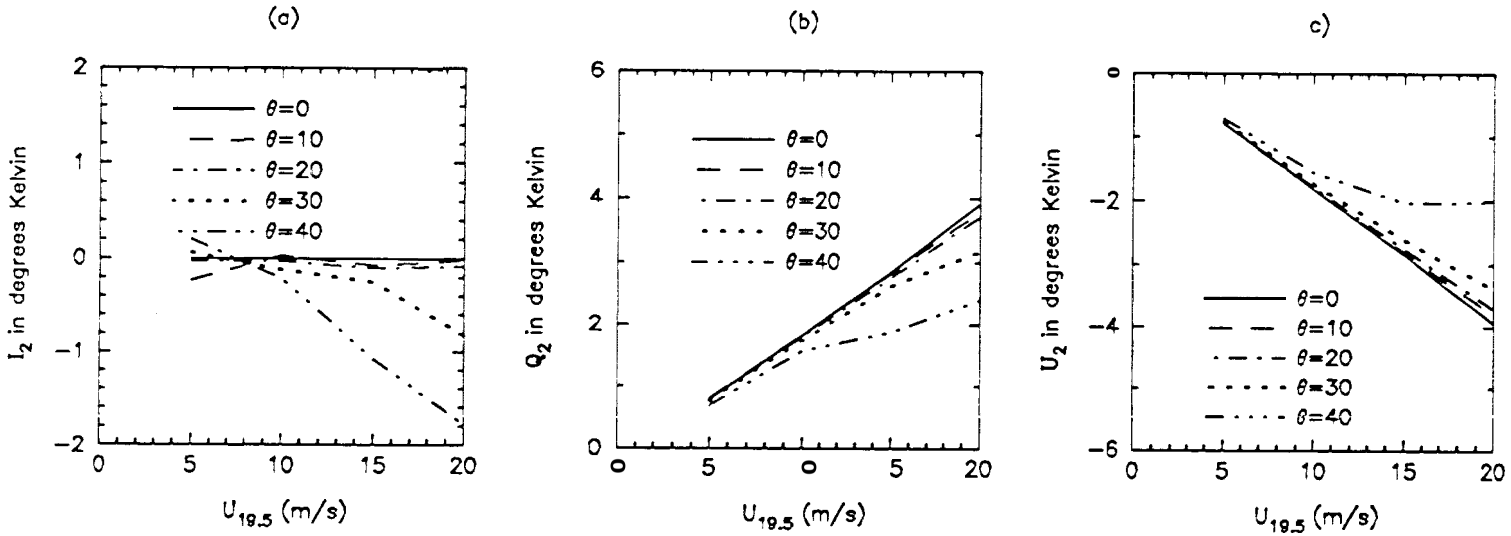
(a)
(b)
c)
I_2 in degrees Kelvin
Q_2 in degrees Kelvin
U_2 in degrees Kelvin
$U_{19.5}$ (m/s)
θ=0
θ=10
θ=20
θ=30
θ=40